New & Renewable Energy 2026. 3 Vol. 22, No. 1
ISSN 1738-3935 (Print)
ISSN 2713-9999 (Online)
https://doi.org/10.7849/ksnre.2026.2046

[2026-3-HP-011]

3 kW급 펌프수차 모델의 비정상 S-곡선 특성 개선을 위한 임펠러 블레이드 각도 최적화

쉬레스트 우즈왈[1)] · 최영도[1),2)*]

Optimization of Impeller Blade Angle to Improve Unsteady S-Curve Characteristics in 3 kW-class Pump Turbine Model

Ujjwal Shrestha[1)] · Young-Do Choi[1),2)*]

Received 10 December 2025 **Revised** 26 December 2025 **Accepted** 30 December 2025 **Published online** 12 February 2026

ABSTRACT Pump turbines are essential components in small-scale hydropower systems, enabling both energy generation and water pumping within a single unit. However, their performance is often constrained by instabilities in the S-Curve region, cavitation, and pressure fluctuations, particularly under off-design conditions. This study aims to optimize the impeller blade angle of a 3 kW-class pump turbine to enhance hydraulic performance and mitigate unsteady S-Curve characteristics. A scaled-down model was designed using the discharge-to-head gradient method and analyzed through experimental testing and computational fluid dynamics simulations with the shear stress transport turbulence model. A multi-objective genetic algorithm-based optimization was used to refine the blade angle distribution at the hub and shroud sections. The results indicate that the optimized impeller increases efficiency in both pump and turbine modes, reduces the S-Curve steepness, suppresses cavitation, and minimizes pressure fluctuations at blade-passing frequencies. These findings demonstrate that blade angle optimization is an effective strategy for improving the operational stability and reliability of pump turbine systems.

Key words Pump turbine(펌프수차), Impeller blade angle(임펠러 블레이드 각도), Shape optimization(형상 최적화), S-Curve characteristics(S-곡선 특성), Cavitation(캐비테이션), Pressure fluctuation(압력 변동)

Nomenclature

BPF : blade passing frequency, Hz
D : reference diameter, m
d_{imp} : impeller design variables
f_n : runner rotational frequency, Hz
$f_{\overline{X}}$: uncertainty error, %
H : effective head, m
LE : leading edge
N : rotational speed, min^{-1}
N_{11} : unit speed
N_s : specific speed
n : total number of measured data
p : static pressure, Pa
P : shaft power, kW

---

1) Academic Research Professor, Institute of New and Renewable Energy Technology Research, Mokpo National University

2) Professor, Department of Mechanical Engineering, Mokpo National University

***Corresponding author:** ydchoi@mnu.ac.kr
Tel: +82-61-450-2419 Fax: +82-61-452-6376

Q : flow rate, m^3/s
Q_{11} : unit discharge
TE : trailing edge
TKE : turbulence kinetic energy, m^2/s^2
U : uncertainty in the measurement data
u : velocity, m/s
u_x : velocity in x-direction, m/s
u_y : velocity in y-direction, m/s
u_z : velocity in z-direction, m/s
X_i : measured data at the i^{th} location
X_{max} : maximum value in measurement data
X_{min} : minimum value in measurement data
z : number of impeller blades
ΔH : head loss, m
$\overline{X}$: mean of measured data
α : guide vane opening angle, °
β : impeller blade angle, °
γ : flow uniformity, %
δ : S-Curve steepness, °
η : efficiency, %
σ : cavitation number
σ_s : standard deviation of measured data
ω : vorticity, s^{-1}

Subscript

1 : leading edge in pump mode
5 : trailing edge in pump mode
h : impeller hub
in : impeller inlet in pump mode
L : lower bound
p : pump mode
s : impeller shroud
t : turbine mode
U : upper bound
vap : vapor pressure at atmospheric pressure

1. Introduction

Pumped-storage hydropower has emerged as a cornerstone technology in modern energy systems, providing large-scale energy storage and enhancing grid stability amid increasing renewable energy penetration. Globally, pumped-storage plants account for over 90% of grid-scale energy storage capacity, providing essential services such as peak load shifting, frequency regulation, and emergency backup power.[1,2] At the heart of these systems lies the pump turbine—a reversible hydraulic machine capable of operating alternately in pump and turbine modes. This dual functionality enables efficient energy transfer between the reservoirs, making pump turbines indispensable for hybrid renewable energy systems and micro-hydropower applications in remote regions.[3,4]

Despite their advantages, pump turbines face significant operational challenges, particularly under off-design conditions. One of the most critical issues is the occurrence of S-Curve characteristics in turbine mode, which induces hydraulic instability during transient processes such as start-up and load rejection.[5,6] These instabilities manifest as severe pressure fluctuations, rotor-stator interactions, and rotating stall phenomena, compromising both efficiency and structural integrity.[7] Cavitation is the formation and collapse of vapor bubbles in low-pressure regions, which further threaten reliability by causing erosion, vibration, and noise.[8,9] Studies have shown that cavitation intensity and pressure pulsation amplitude increase significantly in the S-Curve region, further exacerbating instability.[10,11]

Recent research has focused on mitigating these issues through geometric optimization and advanced computational techniques. Bhukya *et al.*[12] and Du *et al.*[13] investigated blade parameter optimization, including wrap angle and thickness, to enhance hydraulic performance. Guo *et al.*[14] proposed optimal design strategies for micro reversible pump turbines to balance generation and storage modes, while Yang *et al.*[15] compared blade profiles to improve efficiency. CFD-based studies, combined with experimental validation, have confirmed the effectiveness of blade geometry optimization in reducing pressure pulsations and enhancing overall performance.[16,17] Multi-objective optimization algorithms, such as genetic algorithms (GA), have been increasingly adopted in turbomachinery design, enabling simultaneous consideration of conflicting objectives — such as maximizing efficiency while minimizing pressure fluctuations—within constrained design spaces.[18~20]

While previous works have addressed blade geometry and cavitation suppression, this study introduces a targeted approach by optimizing impeller blade angle distribution at both hub and shroud sections for a 3 kW-class pump turbine, which is crucial for small-scale hydropower and hybrid renewable systems. The proposed methodology integrates experimental validation, CFD simulations, and GA-based multi-objective optimization to simultaneously enhance hydraulic efficiency, suppress cavitation, and improve S-Curve stability. This comprehensive framework ensures robust design improvements and operational reliability for micro-hydropower applications.

2. Design and Analysis Methodology

2.1 Design of scale-down pump turbine model

A scaled-down pump turbine model was developed for performance investigation and internal flow analysis. Eqs. (1) and (2) are used to calculate the pump turbine specific speed in pump mode and turbine mode, which are 31.1 [m-m^3/s] and 109.6 [m-kW], respectively. The rotational speed of the pump turbine is 1,800 min^{-1} for pump and turbine modes. The effective heads and flow rates for the pump mode and turbine mode are H_p = 16.5 m, Q_p = 0.020 m^3/s, and H_t = 15m, Q_t = 0.026 m^3/s, respectively. The design specification of the 3 kW class pump turbine model is shown in Table 1. The meridional shape and 3D model of the pump turbine are shown in Fig. 1 according to the pump mode. The meridional shape is for a low specific speed pump turbine. Hence, the ratio of outlet diameter to inlet diameter is higher, and the ratio of outlet width to inlet diameter is lower than the higher specific pump turbine. The inlet and outlet diameters of the pump turbine are 112 mm and 198 mm, respectively, in pump mode. According to the pump mode, the outlet width of the pump turbine impeller is 15.2 mm. 5 impeller blades with 14 guide vanes are used for the pump turbine modes.

$$N_{s_p} = \frac{N\sqrt{Q_p}}{H_p^{0.75}} \tag{1}$$

$$N_{s_t} = \frac{N\sqrt{P_t}}{H_t^{1.25}} \tag{2}$$

Table 1. Design parameters of a 3 kW-class pump turbine model

Parameter	Pump Mode	Turbine Mode
Head, H (m)	16.5	15
Flow rate, Q (m^3/s)	0.020	0.026
Rotational speed, N (min^{-1})	1800	
Shaft Power, P (kW)	3.13	3.23
Specific Speed, N_s	31.1 [m-m^3/s]	109.6 [m-kW]
Reference Diameter, D (m)	0.198 m	

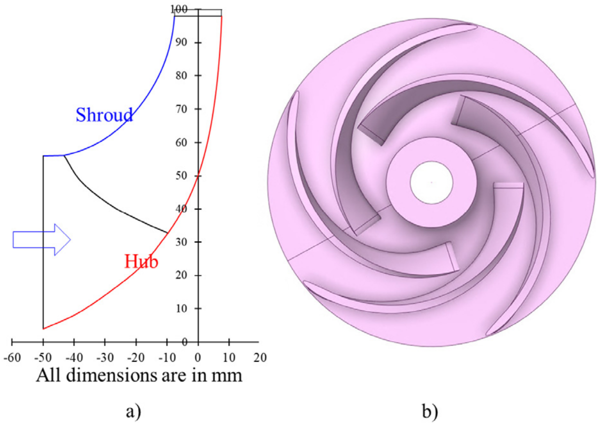

a)

b)

Fig. 1. a) Meridional shape based on pump mode and b) 3D modeling of a 3 kW-class pump turbine model

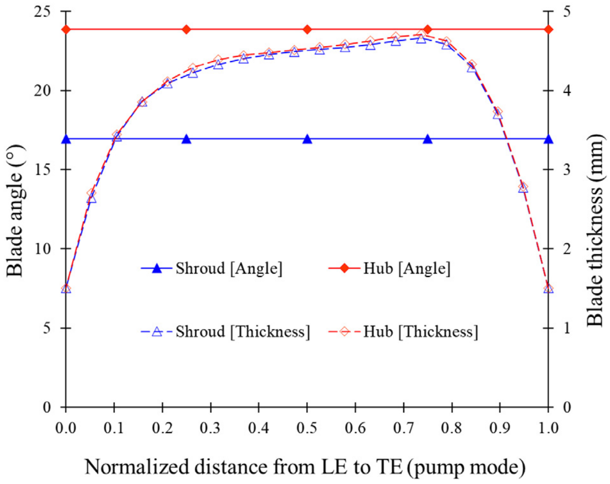

Fig. 2. Blade angle and thickness distribution of scale-down pump turbine model

The blade angle and thickness distribution for the pump turbine design are indicated in Fig. 2. A constant blade angle distribution was selected for the design of a scaled-down pump turbine. The thickness distribution is shown in Fig. 2 with a maximum thickness of 5 mm. The various impeller designs were prepared using the blade angle distribution.

2.2 Experimental Methodology

The experimental configuration of the scaled-down pump turbine illustrated in Fig. 3 comprises several essential components: the pump turbine, water tank, centrifugal pump, control valves, flow meter, braking system, motor, pressure sensors, pipe straightener, electronic control panel, and data acquisition system.

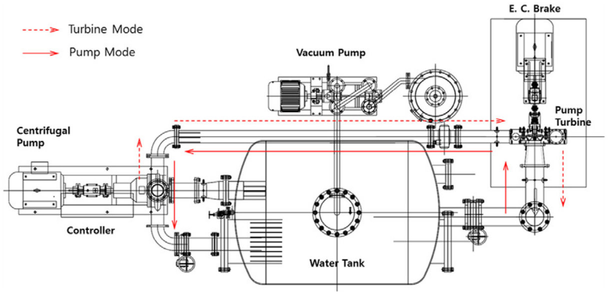

Fig. 3. Experimental setup for the scale-down pump turbine model

The water tank is partitioned into two sections to segregate the inlet and outlet flows; a vacuum pump then evacuates air from the tank to ensure a stable operating pressure. In turbine mode, the centrifugal pump delivers the inlet flow, with a pipe straightener employed to achieve uniform and streamlined flow at the turbine inlet. The discharged flow is subsequently returned to the water tank, closing the loop. Control valves in the facility regulate both the hydraulic head and volumetric flow rate. An electromagnetic flowmeter records the flow rate, while pressure taps located at multiple points provide pressure measurements. Torque and rotational speed are monitored via a transducer positioned between the turbine and dynamometer. The dynamometer acts as an electronic generator to control turbine torque and speed, and excess thermal energy generated during braking is dissipated by an air-cooling system. In pump mode, the dynamometer is replaced by a motor; however, practical applications use a synchronous motor generator instead.

Table 2 shows the result of the error and uncertainty analysis in measurement, which are calculated using Eqs. (3)-(6). The uncertainty in the measurement of efficiency is 1.6%. The uncertainty errors of head, flow rate, torque, rotational speed, and efficiency are 0.2523%, 0.0426%, 0.9657%, 0.0706%, and 0.9456%, respectively. The range of error is very small. Therefore, this indicates the precision and accuracy of the measurement are quite reliable.

Table 2. Uncertainty analysis of 3kW-class pump turbine in turbine mode

	Units	$\overline{X}$	σ_s	U	$f_{\overline{X}}$
Flow	m^3/s	0.0309	0.000013	0.000021	0.0426%
Torque	kgfm	1.7401	0.0168	0.0372	0.9657%
Speed	min^{-1}	1797.08	1.2685	2.5080	0.0706%
Head	m	15.1297	0.0382	0.0883	0.2523%
Pressure	kgf/cm^2	1.5303	0.0038	0.0094	0.2512%
Efficiency	%	82.7043	0.7556	1.6409	0.9456%

$$\overline{X} = \frac{\sum_{i=1}^{n} X_i}{n} \tag{3}$$

$$\sigma_s = \sqrt{\sum_{i=1}^{n} \frac{\left(X_i - \overline{X}\right)^2}{n-1}} \tag{4}$$

$$\pm U = \frac{X_{\max} - X_{\min}}{2} \tag{5}$$

$$f_{\overline{X}} = \frac{\sigma_s}{\overline{X}} \times 100\% \tag{6}$$

2.3 Numerical Methodology

ANSYS 2022R2 was employed for the CFD analysis of a scaled-down pump turbine model. Reynolds Averaged Navier Stokes (RANS) equations were used to perform incompressible flow simulations. A two-equation RANS model with shear stress transport (SST) turbulence closure was adopted for the detailed numerical investigation of the pump turbine. The SST turbulence model was selected to improve the accuracy of torque and efficiency predictions. The present study focuses on the S-Curve characteristic behavior of the pump turbine. A high-resolution scheme was applied to both the advection and turbulence terms. The convergence criterion was set to 10^{-6} for the residuals. The reliable simulations were achieved using high-quality numerical grids. ANSYS ICEM 2022R2 was used to generate hexahedral structured grids for the numerical analysis. Fig. 4 illustrates the computational grid employed in the turbine simulations. The boundary conditions applied to the pump turbine are summarized in Table 3. In pump mode, the inlet and outlet were specified as static pressure and mass flow rate, respectively. In turbine mode, total pressure and static pressure were imposed at the inlet and outlet, respectively. Fig. 5 shows the mesh dependency test with 6.6 million nodes and $y^+ < 5$ on impeller blades, which exhibited the minimum change in the normalized efficiency.

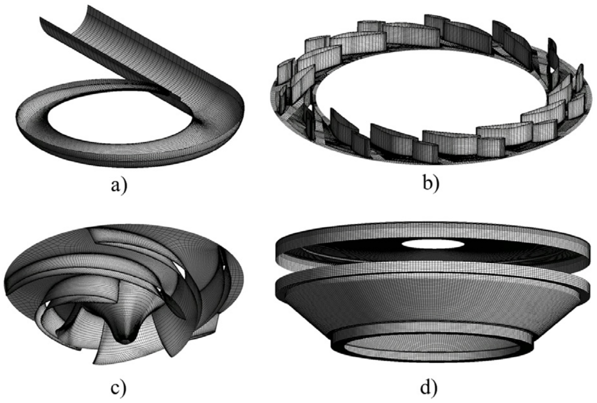

Fig. 4. Numerical grids for scale-down pump turbine mode

Table 3. Boundary conditions for CFD analysis of scale-down pump turbine model

Parameter	Condition/Value	
	Turbine Mode	Pump Mode
Analysis Type	Steady and Unsteady State	
Inlet	Total Pressure	Static Pressure
Outlet	Static Pressure	Mass Flow rate
Rotational speed	1800 min^{-1}	
Turbulence model	Steady – SST Unsteady – SAS-SST	
Physical time scale	Steady - 0.0053 s	
Time steps	Unsteady – 0.0001 s	
Interface model	Steady - Frozen rotor Unsteady - Transient rotor stator	

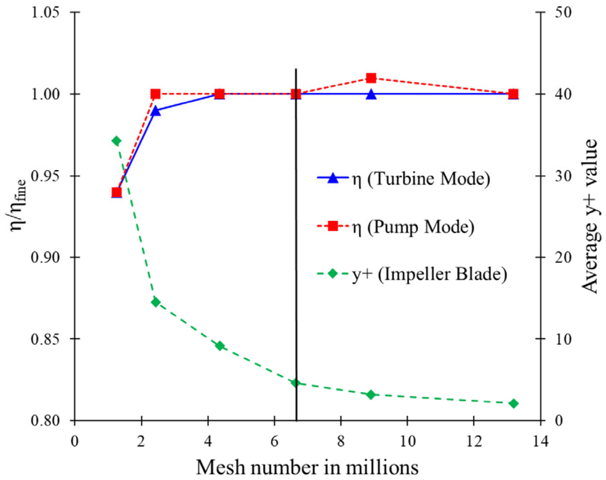

Fig. 5. Mesh dependency test for pump turbine model CFD analysis

2.4 Optimization Methodology

Optimization in turbomachinery is a demanding task due to the complex flow phenomena and interactions between rotating and stationary components. Fig. 6 illustrates the flowchart for impeller shape optimization. The multi-objective genetic algorithm (MOGA) is considered the most suitable approach for optimization of the design parameters. The blade angle (β) is chosen as the design variable, with five points each on the hub and shroud lines. Consequently, there are 10 design variables for the impeller blade angle, as shown in Fig. 2. The design variable d_{imp} is defined in Eq. (7). The lower and upper bounds for the impeller design variables are presented in Table 4. These bounds are selected to satisfy the pump turbine design requirements. Typically, the inlet and outlet angles for a pump-turbine range from 15° to 30° and 12° to 25° in the pump mode.[21,22]

The optimization formulation for the impeller shape design is provided in Eq. (8), and the MOGA settings are summarized in Table 5.

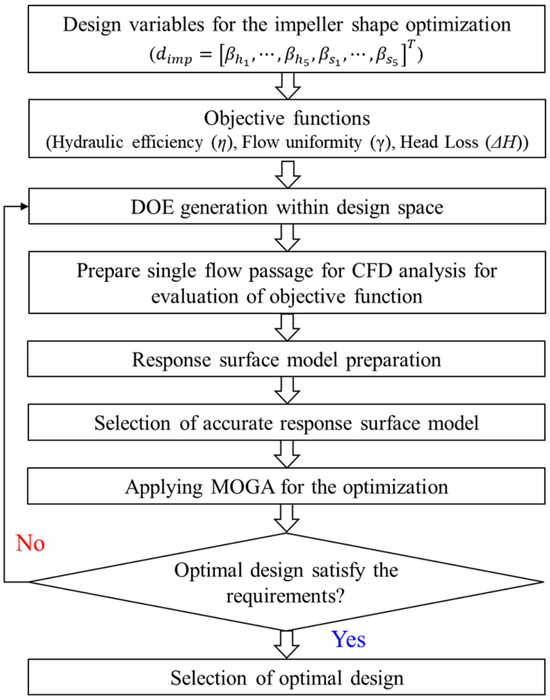

Fig. 6. Optimization methodology for the impeller shape optimization

Table 4. Lower and upper bounds for impeller design variables

Design Variables	Lower Bound (d_{imp}^L)	Upper Bound (d_{imp}^U)	Initial Design
β_{h_1}	15°	30°	23.87°
β_{h_2}	20°	45°	23.87°
β_{h_3}	20°	45°	23.87°
β_{h_4}	20°	45°	23.87°
β_{h_5}	15°	30°	23.87°
β_{s_1}	10°	22°	16.95°
β_{s_2}	12°	35°	16.95°
β_{s_3}	12°	35°	16.95°
β_{s_4}	12°	35°	16.95°
β_{s_5}	10°	22°	16.95°

Table 5. Basic setting for impeller blade optimization using MOGA

Paameter	Value
Initial Sampling	Optimal Space Filling
Maximum number of cycle	20
Number of initial samples	100
Number of samples per iteration	50
Maximum number of generations	50
Convergence stability percentage	1%
Mutation Probability	2%
Crossover Probability	98%

$$d_{imp} = \left[\beta_{h_1}, \ldots, \beta_{h_5}, \beta_{s_1}, \ldots, \beta_{s_5}\right]^T \tag{7}$$

$$\begin{aligned} & maximize\ \ \eta(d_{imp}), \gamma(d_{imp}) \\ & minimize\ \ \Delta H(d_{imp}) \\ & subject\,to\ 12m \le H(d_{imp}) \le 16m \\ & \qquad 0.018\,m^3/s \le Q(d_{imp}) \le 0.028\,m^3/s \\ & \qquad \eta(d_{imp}) \ge 80\% \\ & \qquad d_{imp}^L \le d_{imp} \le d_{imp}^U \end{aligned} \tag{8}$$

3. Results and Discussion

3.1 Experimental Validation

The experiment was conducted for a pump turbine in both pump and turbine modes. The unit discharge and unit speed are used for the performance analysis.

$$N_{11} = \frac{ND}{\sqrt{H}} \tag{9}$$

$$Q_{11} = \frac{Q}{D^2\sqrt{H}} \tag{10}$$

Figure 7 presents the performance curves in pump mode. The pump–turbine achieves its best efficiency of 83% at a head of 16 m, with a power consumption of 3.33 kW. Fig. 8 compares performance between experimental results and CFD analysis in turbine mode. In turbine mode, the best efficiency is 85% at a head of 15 m, and the output power reaches 3.45 kW, which is higher than the power consumption in pump mode. The experimental and CFD results exhibit good agreement in both pump and turbine modes.

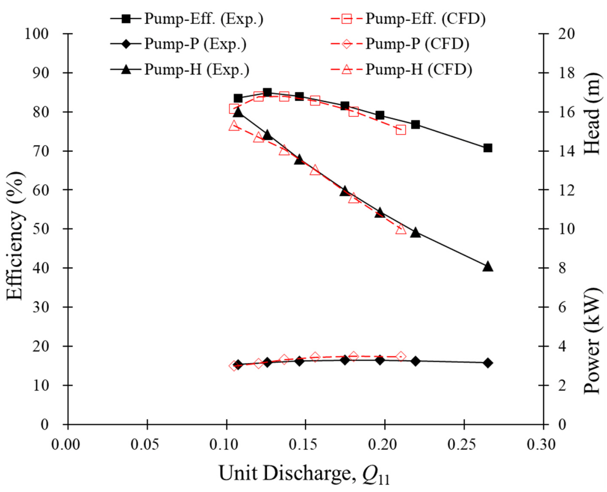

Fig. 7. Comparison of experiment and CFD analysis of scale–down pump turbine model in pump mode

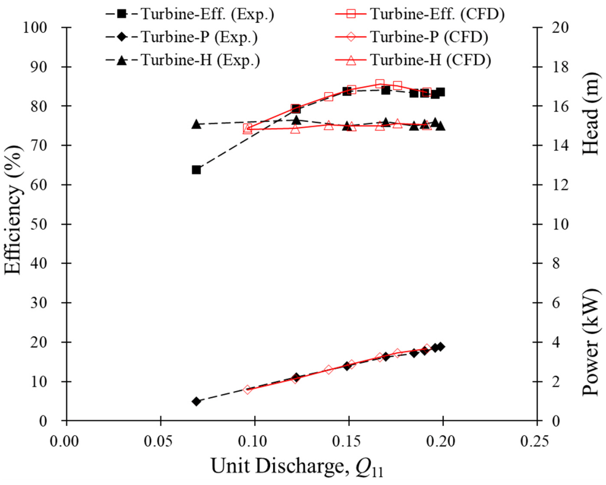

Fig. 8. Comparison of experiment and CFD analysis of scale–down pump turbine model in turbine mode

3.2 Impeller Shape Optimization

The optimal pump turbine is selected based on hydraulic performance and S–Curve characteristics. Fig. 9 shows the Pareto front for the impeller shape optimization. The Pareto front is prepared using flow uniformity in turbine mode at Q_{11} = 0.10 and α = 17° in the x–axis and head loss in pump mode at Q_{11} = 0.16. Fig. 10

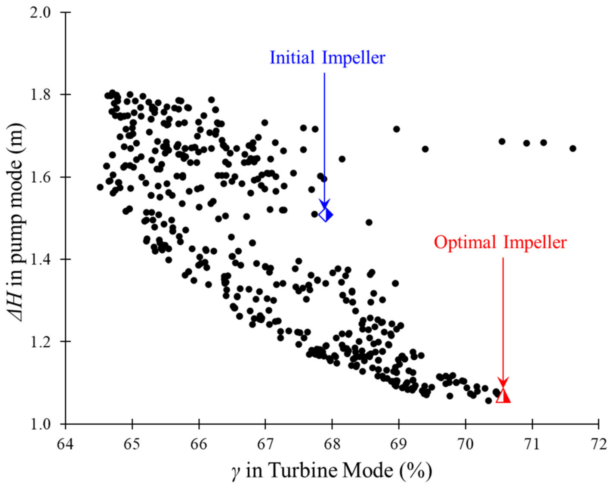

Fig. 9. Pareto Front for the optimization of impeller shape

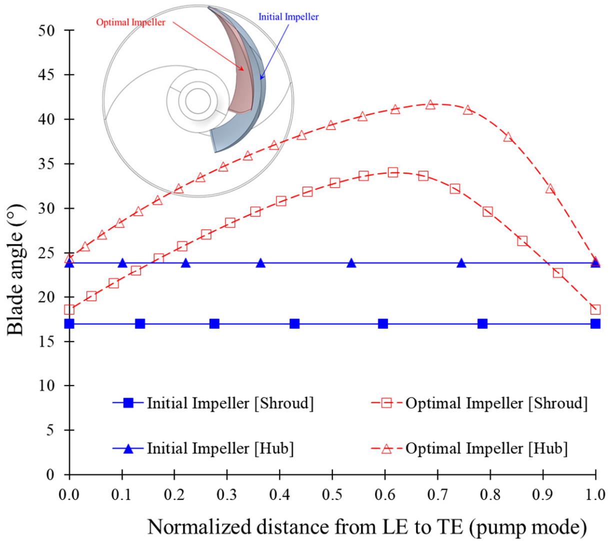

Fig. 10. Comparison of initial and optimal impeller blade angle distribution

compares the initial and optimal impeller shapes and blade angle distributions. The optimization considers the blade angle distribution at the hub and shroud region. The constant blade angle distribution is selected for the initial impeller design. While optimizing, the blade angle distribution is considered to improve the hydraulic performance and the S–Curve characteristics. The optimal impeller exhibits blade angles of 41° and 34° at 0.7 normalized distance from LE in pump mode at the hub and shroud sections. The blade angle increases from 0.0 to 0.7 and then decreases from 0.7 to 1.0 normalized distance from LE in pump mode.

3.3 Comparison between Initial and Optimal Impeller Shape Performance

Figure 11 illustrates the performance curves of the pump turbine in pump mode. The maximum efficiencies of the initial and optimized impellers are 82.75% and 84.24%, respectively. At partial flow rates, the performance of both impellers is nearly identical. For the optimized impeller at Q_{11} = 0.06, the pump efficiency, head, and power are 68.06%, 16.43 m, and 2.6 kW, respectively. A significant improvement in performance is observed for the optimized impeller when $Q_{11} > 0.13$. At Q_{11} = 0.19, the pump head increases by 16.2%. The performance curves indicate that the head increases significantly at high flow rates with the optimized impeller compared to the initial impeller shape.

Figure 12 compares the pressure contours between the initial and optimized impeller shapes. With the optimized impeller, the outlet pressure in pump mode reaches 215 kPa, compared to 183 kPa for the initial design, indicating a 17% increase at the outlet. Fig. 13 illustrates the pressure distribution from LE to TE of the impeller flow passage in pump mode. The outlet pressure is significantly higher for the optimized impeller. Moreover, the pressure difference between the suction

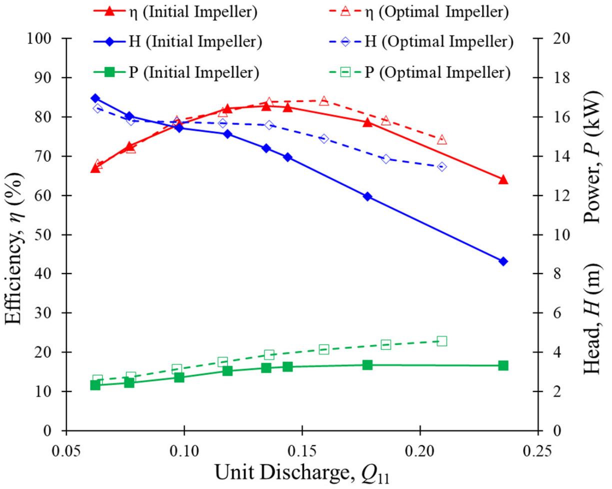

Fig. 11. Comparison of performance curves between the initial and optimal impeller in pump mode

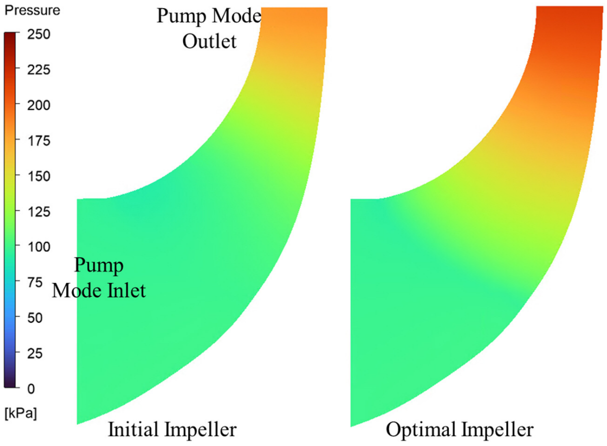

Fig. 12. Comparison of pressure contours in the meridional plane in pump mode at Q_{11}=0.21

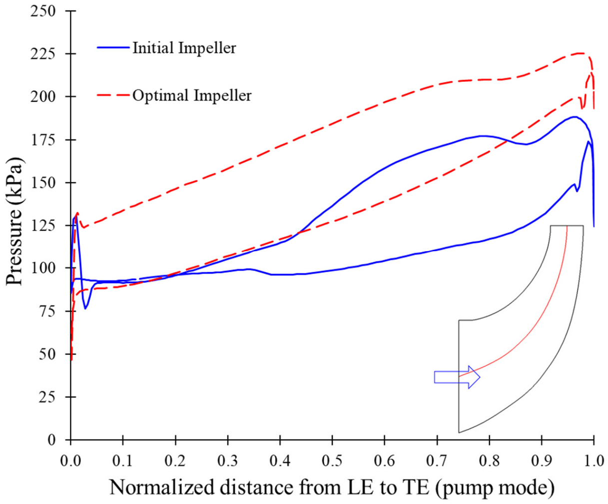

Fig. 13. Comparison of pressure distribution from LE to TE of pump turbine imepller in pump mode at Q_{11}=0.21

and pressure sides remains uniform from inlet to outlet for the optimized shape, unlike the initial design. The blade angle distribution in the optimized impeller contributes to improved outlet pressure, resulting in better pump performance compared to the initial impeller.

Figure 14 shows the turbine mode performance curves for the initial and optimized impellers. The peak efficiencies occur at Q_{11} = 0.18 for the initial impeller and Q_{11} = 0.21 for the optimized impeller. At the best operating point, the optimized impeller increases output power from 3.4 kW to 3.9 kW. However, within the operating range 0.10 ≤ Q_{11} ≤ 0.19, the initial impeller demonstrates superior turbine efficiency and output power.

Figure 15 compares the pressure distribution from LE to TE in turbine mode for initial and optimal impeller shapes. The optimized impeller exhibits a more uniform and smoother pressure difference between the suction and pressure sides, whereas the initial impeller shows a drastic variation. Figs. 16 and 17 compare the turbulence kinetic energy (TKE) between the initial and optimized impellers at the turbine mode inlet. TKE is associated with the eddies in the

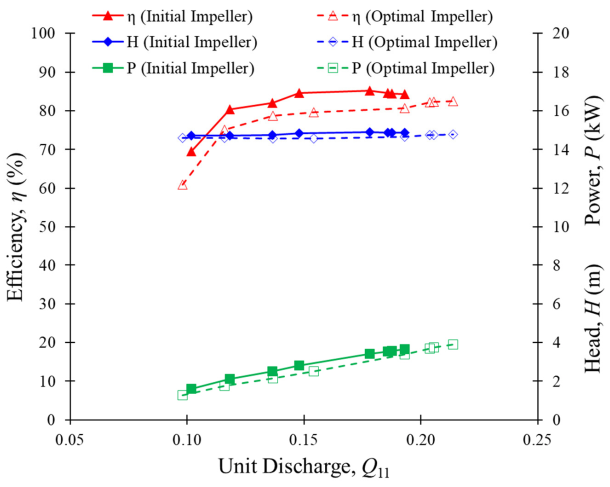

Fig. 14. Comparison of performance curves between the initial and optimal impeller in turbine mode

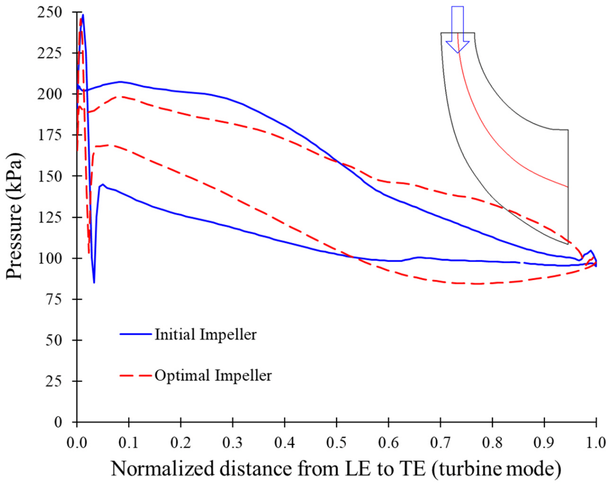

Fig. 15. Comparison of pressure distribution from LE to TE of pump turbine impeller in turbine mode at Q_{11}=0.20

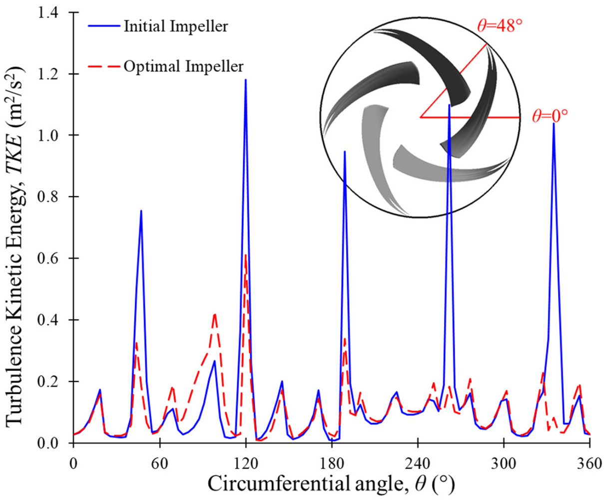

Fig. 16. Comparison of vorticity distribution at turbine mode inlet of pump turbine model at Q_{11}=0.20

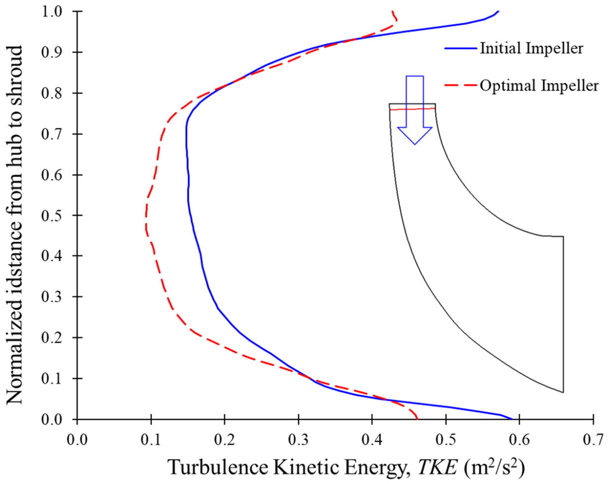

Fig. 17. Comparison of TKE distribution in turbine mode inlet of pump turbine model at Q_{11}=0.20

turbulent flow and is quantified by the mean kinetic energy of velocity fluctuations.

$$TKE=\frac{1}{2}\left(\overline{u_x^2}+\overline{u_y^2}+\overline{u_z^2}\right) \tag{11}$$

A high TKE value indicates a strong velocity gradient, flow separation, intense secondary flow interactions, and increased energy loss. The number of TKE peaks corresponds to the number of impeller blades. Each peak value for the initial impeller exceeds $0.6\ m^2/s^2$. The peak TKE value for the optimized impeller is less than $0.6\ m^2/s^2$ for each blade passage. The maximum TKE magnitude for the optimized impeller is reduced by 48% compared to the initial impeller shape. A high TKE value indicates a strong velocity gradient, flow separation, intense secondary flow interactions, and increased energy loss. The number of TKE peaks corresponds to the number of impeller blades. For the initial impeller, each peak exceeds $0.6\ m^2/s^2$, whereas the optimized impeller maintains values below this threshold, demonstrating a significant reduction in turbulence intensity and eddy formation in the impeller flow passage. Fig. 17 illustrates the TKE distribution from hub to shroud at the turbine–mode inlet. The TKE magnitudes at the hub and shroud walls are 22% and 25% lower, respectively, for the optimized impeller compared to the initial design. Across the normalized span (0.2 – 0.8 from hub to shroud), the distribution remains mostly uniform; however, the optimized impeller exhibits 44% lower TKE intensity than the initial impeller. This reduction in TKE indicates that the optimized impeller effectively suppresses secondary flows, eddies, and pressure pulsations, contributing to improved hydraulic stability and efficiency.

Figure 18 compares the S–Curve characteristics of the initial and optimized impellers. The S–Curve was generated by varying the flow rate at the same guide vane opening in turbine mode, where $\alpha = 0^{\circ}$ represents a fully closed guide vane. For the initial impeller at $\alpha = 13^{\circ}$ and 17°, the curve slope changes sharply from negative to positive, indicating strong S–Curve characteristics. The steepness of the initial impeller's S–Curve at $\alpha = 13^{\circ}$ and 17 is 23° and 37°, respectively. The optimized impeller shape reduces the steepness to 8° and 13° for $\alpha = 13^{\circ}$ and 17°, respectively. At $\alpha = 24^{\circ}$, both the initial and optimized impellers exhibit low steepness values. However, at $Q_{11}=0.06$, the N_{11} values for the initial and optimized impellers are 131.56 and 115.62, respectively, indicating that the effective head for the optimized impeller is higher than that of the initial design. Consequently, the optimized impeller improves S–Curve characteristics by reducing the curve's inclination and increasing the effective head at a constant Q_{11}, thereby enhancing stability and enabling flexible pump turbine operation.

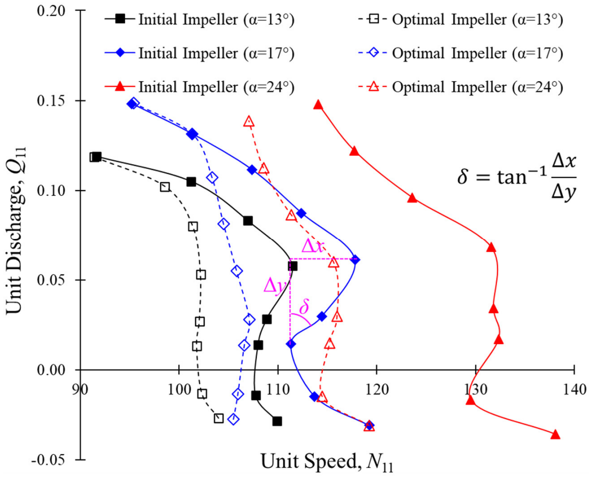

Fig. 18. Comparison of the S–Curve between the initial and optimal impeller in turbine mode

Figure 19 illustrates the comparison of vorticity and TKE in the S–Curve region along the circumferential angle for initial and optimal impeller shapes. The vorticity is the local rotation of the flow caused by wall shear and secondary flow, which is represented by Eq. (12).

$$\omega = \nabla \times u \tag{12}$$

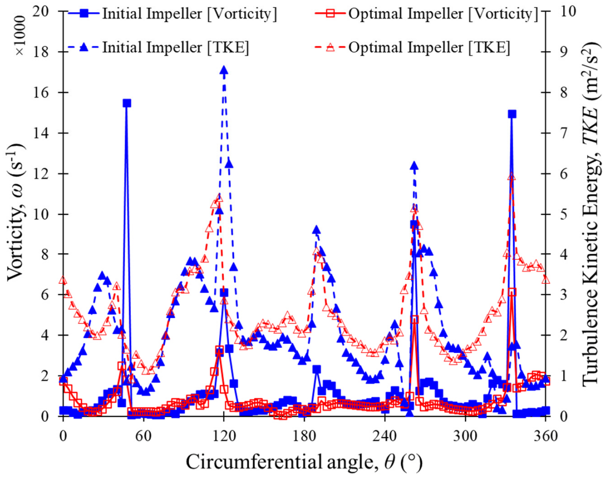

Fig. 19. Comparison of vorticity and TKE distribution at the turbine mode inlet, α=13° and Q_{11}=0.05

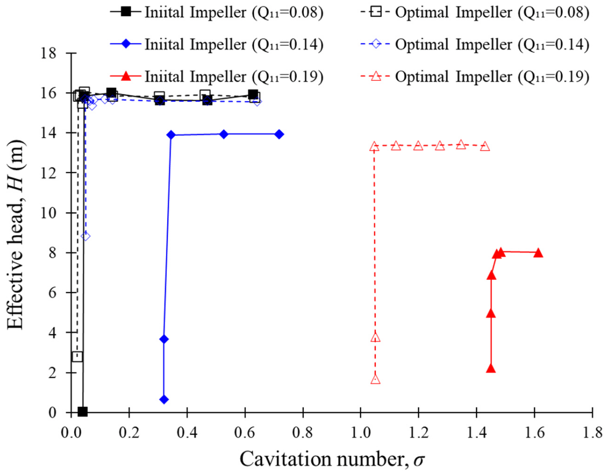

Fig. 20. Comparison of suction performance between the initial and optimal impeller in pump mode

The initial impeller exhibits pronounced peaks in both vorticity and turbulence kinetic energy (TKE) at blade–passing positions, with maximum vorticity approaching 16,000 s^{-1} and TKE reaching approximately 9 m^2/s^2. These peaks indicate vortex formation, intense rotor–stator interactions, and localized turbulence, which contribute to hydraulic instability, pressure pulsations, and energy losses. In contrast, the optimized impeller demonstrates a substantial reduction in peak values, with vorticity limited to 6,100 s^{-1} and TKE reduced to 5 m^2/s^2. Furthermore, the optimized design produces smoother and more uniform distributions of vorticity and TKE across the circumferential domain, suggesting improved flow alignment, reduced secondary flow intensity, and enhanced hydraulic stability. Overall, the reductions in vorticity and TKE by approximately 60% and 30%, respectively, are critical for mitigating unsteady pressure fluctuations, minimizing cavitation risk, and improving S–Curve characteristics.

3.4 Comparison of Cavitation between Initial and Optimal Impeller Shape

The cavitation analysis is performed with an initial and optimal impeller with various cavitation numbers in pump mode. The cavitation number is defined in Eq. (13).

$$\sigma = \frac{(p_{in} - p_{vap})}{\rho g H} \tag{13}$$

Figure 20 compares the suction performance between the initial and optimized impellers in pump mode. The evaluation is based on the critical cavitation number, which corresponds to the cavitation inception point where the effective head and efficiency decrease by 3% or more. At Q_{11} = 0.08, the critical cavitation numbers for the initial and optimized impellers are 0.03 and 0.02, respectively, with an effective head of 16 m. The cavitation number is very low, resulting in negligible influence on suction performance and a minimal likelihood of cavitation. At Q_{11} = 0.14, the critical cavitation numbers and effective heads for the initial and optimal impellers are 0.32 and 0.05, and 16 m and 14 m, respectively. These results indicate that the initial impeller is more prone to cavitation at this flow rate. Furthermore, at Q_{11} = 0.19, the critical cavitation numbers increase to 1.45 and 1.05 for the initial and optimized impellers, with corresponding effective heads of 13 m and 8 m.

Figure 21 shows the comparison of the vapor volume fraction distribution in the initial and optimal impeller. In legend, 0 refers to water, and 1 refers to water vapor. The vapor volume fraction is reduced significantly

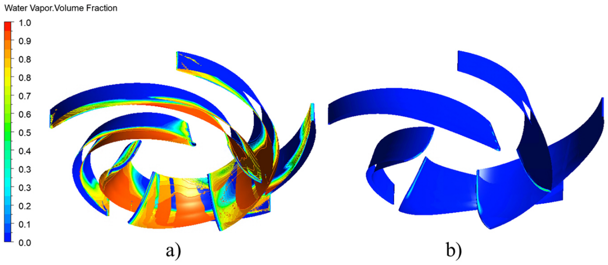

Fig. 21. Volume fraction distribution in a) initial and b) optimal impeller at Q_{11}=0.14 and σ=0.32 in pump mode

with the optimal impeller at Q_{11} = 0.14 and σ = 0.32, confirming that the optimized impeller design is more effective in suppressing cavitation compared to the initial impeller design.

3.5 Comparison of Pressure Fluctuation between Initial and Optimal Impeller Shape

A Fast Fourier Transformation (FFT) is employed to analyze pressure fluctuation in the pump turbine model and to determine the blade passing frequency (BPF) for both the initial and optimal impeller.

$$f_n = \frac{N}{60} \tag{14}$$

$$BPF = zf_n \tag{15}$$

Figure 22 shows the pressure fluctuations at the impeller and guide vane interface (GV 1) at Q_{11} = 0.08 in the S–Curve region. Peak pressure oscillations are observed at integral multiples of the BPF. At BPF, the pressure magnitude decreases from 11.5 kPa to 6.3 kPa with the optimal impeller shape. Similarly, the pressure amplitude at 2BPF is reduced from 8.0 kPa to 5.1 kPa with an optimal impeller shape.

Figure 23 presents the pressure fluctuations at the impeller and guide vane interface (GV 4). At this location, the pressure amplitudes at BPF and 2BPF decrease from 14.9 kPa to 9.5 kPa and from 11.4 kPa to 6.86 kPa, respectively, with the optimal impeller shape. Overall, the pressure amplitudes at integral multiples of BPF are significantly reduced at the impeller–guide vane interface in the S–Curve region. These results confirm that impeller shape optimization effectively suppresses pressure fluctuations within the impeller flow passage. Consequently, the optimized impeller demonstrates improved suction performance, enhanced S–Curve characteristics, and reduced pressure oscillations in the flow passage.

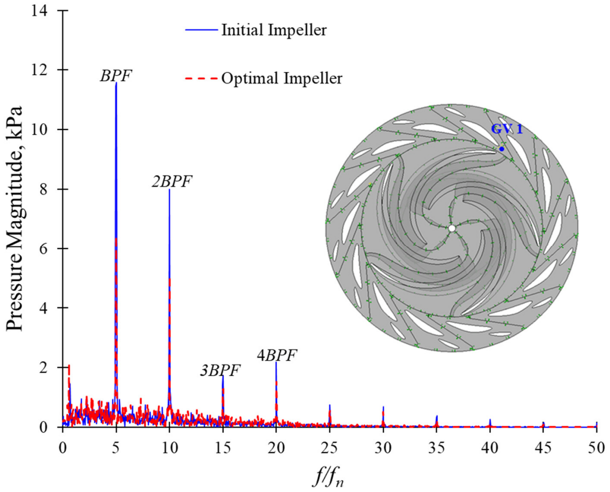

Fig. 22. Comparison of pressure amplitude between initial and optimal impeller in turbine mode at Q_{11}=0.08, α =17° and GV 1

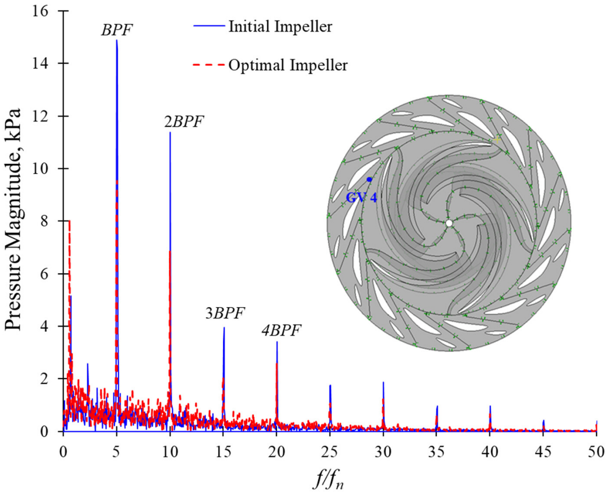

Fig. 23. Comparison of pressure amplitude between initial and optimal impeller in turbine mode at Q_{11}=0.08, α =17° and GV 4

4. Conclusions

This study investigated the optimization of impeller blade angles in a 3 kW-class pump turbine to improve hydraulic performance and mitigate instability in the S-Curve region. Experimental validation and CFD analysis demonstrated good agreement, confirming the reliability of the numerical approach. The optimized impeller, achieved through blade angle distribution at the hub and shroud, resulted in measurable improvements in performance. Specifically, the optimized design increased outlet pressure in pump mode by approximately 17% and enhanced efficiency. In turbine mode, the maximum output power was increased by 15%. Furthermore, turbulence kinetic energy and vorticity peaks in the S-Curve region were reduced by about 30% and 60%, respectively, indicating improved flow uniformity and reduced secondary flow intensity. The optimal impeller shape increased the effective head in turbine mode and reduced the S-Curve steepness by approximately 65% for low guide vane opening. Cavitation analysis confirmed that the optimized impeller lowered the critical cavitation number, improving suction performance under various flow conditions. The optimal impeller reduced pressure fluctuation amplitudes at blade passing frequencies by approximately 30-40%. These findings demonstrate that blade angle optimization is an effective strategy for enhancing performance, suppressing cavitation, and mitigating pressure pulsations in small-scale pump turbine systems.

Acknowledgement

This research was supported by the Regional Innovation System & Education (RISE) program through the Jeollanamdo RISE center, funded by the Ministry of Education (MOE) and the Jeollanamdo, Republic of Korea.(2025-RISE-14- 001).

References

[1] Hu, D., Cheng, Y., Zhang, P., Wang, X., Ding, J., and Zhang, X., 2022, “Distribution features of flow patterns and pressure pulsations of pump turbine in five operating modes on the four-quadrant plane”, Front. Energy Res., **10**, 880293.

[2] Zisos, A., Sakki, G.K., and Efstratiadis, A., 2023, “Mixing renewable energy with pumped hydropower storage: Design optimization under uncertainty and other challenges”, Sustainability, **15**(18), 13313.

[3] Morabito, A., and Hendrick, P., 2019, “Pump as turbine applied to micro energy storage and smart water grids: A case study”, Appl. Energy, **241**, 567-579.

[4] Sun, X., Huang, H., Zhao, Y., Tong, L., Lin, H., and Zhang, Y., 2025, “A Review of Methods for" Pump as Turbine"(PAT) Performance Prediction and Optimal Design”, Fluid Dyn. Mater. Process., **21**(6), 1261-1298.

[5] Pang, S., Zhu, B., Shen, Y., and Chen, Z., 2023, “S-shaped characteristics of pump turbine with large guide vane opening by experimental and numerical analysis”, AIP Advances, **13**(1), 015201.

[6] Wang, Z., Zhu, B., Wang, X., and Qin, D., 2017, “Pressure fluctuations in the S-shaped region of a reversible pump turbine”, Energies, **10**(1), 96.

[7] Deng, Y., Xu, J., Li, Y., Zhang, Y., and Kuang, C., 2022,“Experimental and computational fluid dynamics study of the flow field of a model pump turbine”, Front. Energy Res., **10**, 911874.

[8] Lu, J., Li, J., Zhang, C., Zhou, Y., and He, Y., 2025, “Research on the Cavitation Characteristics of Pump Turbines Based on Mode Decomposition”, Processes, **13**(3), 732.

[9] Fahlbeck, J., Nilsson, H., Arabnejad, M. H., and Salehi, S., 2024, “Performance characteristics of a contra-rotating pump turbine in turbine and pump modes under cavitating flow conditions”, Renew. Energy, **237**, 121605.

[10] Stephen, C., Basu, B., and McNabola, A., 2023, “Performance Analysis of a Pump-as-Turbine Under Cavitating Conditions”, In International School of Hydraulics, Springer Nature Switzerland, Cham, pp. 375-383.

[11] Shang, L., Cao, J., Wang, Z., and Liu, X., 2023, “Hydraulic

characterization of variable-speed pump turbine under typical pumping modes", Processes, **11**(10), 2903.

[12] Bhukya, N. K., Sharma, G. K., and Rai, A. K., 2024, "Blade parameter optimization in Pump As Turbine (PAT)", In International Conference on Renewable and Clean Energy, Springer Nature Singapore, Singapore, pp. 3-12.

[13] Du, J., Yang, H., and Shen, Z., 2018, "Study on the impact of blades wrap angle on the performance of pumps as turbines used in water supply system of high-rise buildings", Int. J. Low-Carbon Technol., 1**3**(1), 102-108.

[14] Guo, T., Pan, J., Tao, R., and Xiao, R., 2025, "Optimal Design of a Micro Reversible Pump Turbine for Balancing Generation Mode and Storage Mode", Energy Sci. Eng., **13**(4), 1995-2010.

[15] Yang, S., Zhou, X., Singh, P., Zhou, L., Dong, L., and Li, Y., 2025, "Performance comparison between forward curved blade impeller and backward curved blade impeller in mixed-flow pump-as-turbine", Phys. Fluids, 37, 035113.

[16] Plua, F., Hidalgo, V., Cando, E., Pérez-Sánchez, M., and López Jiménez, P.A., 2022, "Pumps as Turbines (PATs) by Analysis with CFD Models", Int. J. Adv. Sci. Eng. Inf. Technol., **12**(3), 1098-1104.

[17] Abbas, N.J., Quon, E., Iavornic, C., and Obermeyer, H., 2019, "Computational Fluid Dynamics Modeling and Verification of a Submersible pump turbine Runner", National Renewable Energy Laboratory (NREL), NREL/CP-5000-74121, https://docs.nrel.gov/docs/fy20osti/74121.pdf.

[18] Wang, T., Lei, L., Liu, Y., Guo, Q., and Huang, T., 2024, "Effect of blade profile on the hydraulic performance of a double-suction centrifugal pump as turbine based on enstrophy dissipation theory", Phys. Fluids, **36**(8), 085147.

[19] Wang, X. D., Hirsch, C., Kang, S., and Lacor, C., 2011, "Multi-objective optimization of turbomachinery using improved NSGA-II and approximation model", Comput. Methods Appl. Mech. Eng., **200**(9-12), 883-895.

[20] Fuhrer, C., Kovachev, N., Vogt, D.M., Raja Mahalingam, G., and Mann, S., 2024, "Multi-objective numerical optimization of radial turbines", J. Turbomach., **146**(3), 031004.

[21] Olimstad, G., Nielsen, T., and Børresen, B., 2012, "Dependency on runner geometry for reversible-pump turbine characteristics in turbine mode of operation", J. Fluids Eng., **134**(12), 121102.

[22] Ruan, H., Chao, W., Li, X., Zhang, Q., Qing, L. and Wei, C., 2025, "The Influence of the Installation Angle of a Blade's Low-Pressure Edge on the Cavitation Performance of Francis Pump-Turbines", Fluids, **10**(9), 248.